THE JOURNAL OF BIOLOGICAL CHEMISTRY VOL. 282, NO. 37, pp. 27503–27517, September 14, 2007

Cellular Internalization of Green Fluorescent Protein Fused with Herpes Simplex Virus Protein VP22 via a Lipid Raft-mediated Endocytic Pathway Independent of Caveolae and Rho Family GTPases but Dependent on Dynamin and Arf6*[S]

Received for publication, May 9, 2007, and in revised form, July 2, 2007 Published, JBC Papers in Press, July 20, 2007, DOI 10.1074/jbc.M703810200

Kenji Nishi[1] **and Kaoru Saigo**[2]

From the Department of Biophysics and Biochemistry, Graduate School of Science, University of Tokyo, 7-3-1 Hongo, Bunkyo-ku, Tokyo 113-0033, Japan

VP22 is a structural protein of the herpes simplex virus and has been reported to possess unusual trafficking properties. Here we examined the mechanism of cellular uptake of VP22 using a fusion protein between the C-terminal half of VP22 and green fluorescent protein (GFP). Adsorption of VP22-GFP onto a cell surface required heparan sulfate proteoglycans and basic amino acids, in particular, Arg-164 of VP22. Inhibitor treatment, RNA interference, expression of dominant-negative mutant genes, and confocal microscopy all indicated that VP22-GFP enters cells through an endocytic pathway independent of clathrin and caveolae but dependent on dynamin and Arf6 activity. As with CD59 (a lipid raft marker), cell-surface VP22-GFP signals were resistant to Triton X-100 treatment but only partially overlapped cell-surface CD59 signals. Furthermore, unlike other lipid raft-mediated endocytic pathways, no Rho family GTPase was required for VP22-GFP internalization. Internalized VP22 initially entered early endosomes and then moved to lysosomes and possibly recycling endosomes.

Short peptides and protein domains capable of transducing cargo across the plasma membrane are called protein transduction domains (PTDs)[3] (reviewed in Refs. 1 and 2). A short basic peptide from the TAT protein, a transcription activator of human immunodeficiency virus type 1 (3–5), and the third helix of the *Drosophila* Antennapedia homeodomain (6) are widely used as short peptide-type PTDs. Recent experiments showed that these short peptide-type PTDs and the proteins associated with them are most likely to be incorporated into cells via some endocytic mechanism (7, 8).

Endocytosis is a complex mechanism involving numerous protein-protein and protein-lipid interactions (9) and may occur as clathrin-dependent endocytosis, macropinocytosis, caveola-mediated endocytosis, and lipid raft-dependent/caveola-independent endocytosis (9, 10). TAT and TAT-PTD fusion proteins are capable of interacting with negatively charged plasma membrane (11, 12), but their endocytic mechanism differs considerably depending on cell type or protein moieties associated with TAT-PTD (12–18). In some cases, they are internalized via macropinocytosis (13, 14), whereas in other cases, they appear to be incorporated into cells via caveola-dependent endocytosis (15, 16) or clathrin-dependent endocytosis (12, 18). Endosomal escape of TAT-PTD fusion proteins may require endosome acidification and cytosolic Hsp90 activity (18–20).

VP22 is a major component of the herpes simplex virus type 1 tegment and is situated between the capsid and envelope (21). This component has been shown to be secreted from cells expressing it through a Golgi-independent mechanism (22). The C-terminal half of VP22, residues 159–301 (termed VP22.C1), is highly homologous in sequence to counterparts of other α-herpes virus VP22 proteins and is considered to be associated with intercellular trafficking ability (23, 24). Although others have reported that a 34-amino acid C-terminal region of VP22.C1 is necessary and sufficient for cellular internalization (25), our results indicate that the entire 142-amino acid region is involved in cellular uptake.[4]

VP22.C1 has been noted to form complexes with fluorescein-labeled oligonucleotides and generate particles of 0.3–1 μm in diameter (24). These particles are efficiently taken up into cultured cells or mice and release active antisense oligonucleotide reagents into the cytoplasm in response to light activation (24, 26, 27). The uptake of VP22.C1-fused green fluorescent protein (GFP), hereafter referred to as VP22-GFP, into an entire tumor has been observed following peritumoral injection into human pancreatic tumors in SCID mice (28). VP22.C1-Rab9 has been reported to be internalized into cells and to exhibit biological activity (29). Thus, as with short peptide-type TAT-PTD, the

* This work was supported in part by a special coordination fund for promoting science and technology and by grants from the Ministry of Education, Culture, Sports, Science and Technology of Japan (to K. S.). The costs of publication of this article were defrayed in part by the payment of page charges. This article must therefore be hereby marked "*advertisement*" in accordance with 18 U.S.C. Section 1734 solely to indicate this fact.

[S] The on-line version of this article (available at http://www.jbc.org) contains supplemental Figs. 1–3.

[1] To whom correspondence may be addressed. Tel.: 81-3-5841-3044; Fax: 81-3-5841-3044; E-mail: kennishi@biochem.s.u-tokyo.ac.jp.

[2] To whom correspondence may be addressed. Tel.: 81-3-5841-3044; Fax: 81-3-5841-3044; E-mail: saigo@biochem.s.u-tokyo.ac.jp.

[3] The abbreviations used are: PTDs, protein transduction domains; GFP, green fluorescent protein; MβCD, methyl-β-cyclodextrin; HA, hemagglutinin; DMEM, Dulbecco's modified Eagle's medium; PBS, phosphate-buffered saline; RNAi, RNA interference; siRNAs, small interfering RNAs; GAG, glycosaminoglycan.

[4] K. Nishi and K. Saigo, unpublished data.

142-amino acid VP22.C1 protein may possibly serve as a vector for delivering cargo into cells. As in the case of TAT-PTD and its fusion proteins, VP22.C1 fusion proteins may also enter a cell via endocytosis because they exhibit cytoplasmic vesicular distribution (8). To date, the cellular internalization mechanism of VP22 fusion proteins is but little understood.

In this work, we studied the mechanism of cellular internalization of VP22 using VP22-GFP as a model system. VP22-GFP was internalized through interactions with cell-surface heparan sulfate proteoglycans and subsequent lipid raft-mediated endocytosis independent of clathrin, caveolae, and Rho family GTPases but dependent on dynamin and Arf6 (ADP-ribosylation factor 6). Also, as with transferrin internalized via clathrin-dependent endocytosis, nearly all internalized VP22-GFP signals were incorporated into the early endosomes and co-localized with transferrin.

EXPERIMENTAL PROCEDURES

Drugs and Antibodies—Alexa Fluor 647-labeled transferrin, phalloidin-labeled rhodamine, and Hoechst 33342 were purchased from Molecular Probes. Heparin (porcine intestinal mucosa), chlorpromazine hydrochloride, methyl-β-cyclodextrin (MβCD), genistein, and *Clostridium difficile* toxin B were obtained from Sigma. Cytochalasin D, okadaic acid, PP2, and sodium orthovanadate were from Calbiochem, and chloroquine diphosphate salt was from Wako. Chondroitin sulfate A (whale cartilage), chondroitin sulfate B (pig skin), chondroitin sulfate C (shark cartilage), keratan sulfate (bovine cornea), heparitinase, and chondroitinase ABC were from Seikagaku Corp. The antibodies used were as follows: anti-heparan sulfate monoclonal antibody (clone NAH46; Seikagaku Corp.); rabbit anti-hemagglutinin (HA) tag polyclonal IgG and goat anti-mouse IgM rhodamine (Upstate); mouse anti-c-Myc monoclonal IgG (Oncogene); anti-Myc tag polyclonal antibody (Cell Signaling Technology); mouse anti-human clathrin heavy chain monoclonal antibody (Affinity BioReagents); anti-CD71 antibody (transferrin receptor; Santa Cruz Biotechnology, Inc.); rabbit anti-EEA1 polyclonal IgG (Upstate); mouse anti-EEA1 monoclonal antibody and anti-human CD107a (LAMP1) antibody (Pharmingen); anti-human CD59 monoclonal antibody (Cedarlane Laboratories); rabbit anti-caveolin-1 polyclonal antibody and mouse anti-GM130 monoclonal antibody (BD Transduction Laboratories); Cy3- or Cy5-conjugated goat anti-mouse IgG (Amersham Biosciences); and fluorescein isothiocyanate-conjugated goat anti-mouse, Cy5-conjugated goat anti-rabbit, and Cy3-conjugated goat anti-rabbit IgG (Jackson ImmunoResearch Laboratories).

Plasmids and VP22 Mutagenesis—pVP22-GFP, an expression plasmid for VP22-GFP production in *Escherichia coli* cells, was constructed as follows. A 0.6-kb EcoRI/NotI fragment of pEGFP-N3 (Clontech) was inserted into the EcoRI/NotI site of the pVP22/myc-His plasmid (Invitrogen). A fragment encoding the C-terminal half of VP22 (amino acids 159–301) and full-length enhanced GFP was amplified from the plasmid by PCR; digested with NheI and NotI; and inserted into the NheI/NotI site of pET28a (Novagen), which is capable of producing recombinant protein with an N-terminal polyhistidine tag. The following primers were used: 5′-AAATTTGCTAGCACGGCGCCAACCCGATCCAA-3′ and 5′-CGGGTTAGATCTCAATGGTGATGGTGATGATGAC-3′. PCR-based systematic mutagenesis was carried out, and a series of pVP22-GFP derivatives encoding mutants of VP22-GFP were generated.[5] pGFP, a GFP expression plasmid, was constructed by inserting the 0.6-kb EcoRI/NotI fragment of pEGFP-N2 (Clontech) into the EcoRI/NotI site of pET28a.

The pcDNA3-HA-dynamin-2a-WT and pcDNA3-HA-dynamin-2a-K44A constructs (30) were obtained from Kazuhisa Nakayama (Kyoto University). The pcDNA3-myc-Rab5-WT and pcDNA3-myc-Rab5-Q79L constructs (31) were kindly provided by Harald Hirling (Faculté des Science de la Vie). pRK5-myc-Rac1-T17N was obtained from Gary Bokoch (Scripps Research Institute). The pXS-HA-Arf6-Q67L plasmid (32) was kindly provided by Julie G. Donaldson (National Institutes of Health).

Protein Purification—VP22-GFP and GFP were produced using *E. coli* BL21 Star (DE3) cells (Invitrogen) as host. Cells were first grown overnight in L-broth with kanamycin at 37 °C. The overnight culture was diluted 10 times with the same medium, and shaking was continued at room temperature. Isopropyl β-D-thiogalactopyranoside was added to a final concentration of 1 mM at A_{600} = 0.8–1.0. After an additional 12 h of shaking at room temperature, the cell cultures were cooled on ice, and the cells were collected by centrifugation at 4 °C. The pellets were frozen and stored at −20 °C until used. Cells were thawed on ice, resuspended in lysis buffer (50 mM sodium phosphate (pH 8.0) containing 10 mM imidazole and 300 mM NaCl), and disrupted by sonication. The lysate was centrifuged at 12,000 × *g* for 1 h at 4 °C. The supernatant was loaded onto a nickel-nitrilotriacetic acid column (Qiagen Inc.) equilibrated with lysis buffer. The column was washed with lysis buffer and then wash buffer (50 mM sodium phosphate (pH 8.0) containing 20 mM imidazole and 300 mM NaCl) and finally eluted with elution buffer (50 mM sodium phosphate (pH 8.0) containing 250 mM imidazole and 300 mM NaCl). Purified protein was immediately used or frozen in 10% glycerol and stored at −80 °C until used.

Cell Culture and Transfection—Wild-type CHO-K1 and HeLa cells were cultured in Dulbecco's modified Eagle's medium (DMEM) supplemented with 10% fetal calf serum at 37 °C in 5% CO_2. Glycosaminoglycan-deficient (pgsA-745) and heparan sulfate-deficient (pgsD-677) mutant CHO-K1 cells (American Type Culture Collection) were cultured in Ham's F12K medium supplemented with 10% fetal calf serum at 37 °C in 5% CO_2. Transfection was carried out using Lipofectamine 2000 (Invitrogen) according to the manufacturer's instructions. Usually, cells were analyzed within the period of 16–48 h following transfection.

Visualization of Internalized Proteins by Confocal Microscopy—Cells were cultured in 12-well culture plates (Sumitomo Bakelite Co., Ltd.) on a glass coverslip. When cells were treated with drug or protein (VP22-GFP, GFP, or transferrin), the culture medium was replaced with fresh serum-free medium at the protein and/or drug concentrations indicated. The cells were incubated for 1 h and then washed twice with ice-cold phos-

[5] The sequences of the primers used for mutagenesis are available upon request.

phate-buffered saline (PBS). After being fixed with 2–4% paraformaldehyde in PBS for 15 min at room temperature unless indicated otherwise, the cells were washed twice with ice-cold PBS and mounted in VECTASHIELD mounting medium (Vector Laboratories). This was followed by cell visualization with an Olympus Fluoview FV1000 confocal microscopy system. Successive 0.25-μm optical sections were taken using a ×60 objective lens. In some cases, after cells had been incubated on ice, the medium was replaced with fresh medium containing protein(s) at the indicated concentrations. The cells were then placed on ice for 1 h, washed twice with serum-free medium, placed in prewarmed serum-free medium, incubated for a specified period of time, and then visualized as described above. Transferrin internalization was examined by exposing cells to culture medium containing 0.25 μM Alexa Fluor 647-labeled transferrin and observing stained cells under a confocal microscope.

Quantification of Internalized VP22-GFP—Cells were seeded on each well of 12-well culture plates in culture medium containing 10% fetal calf serum. Culturing was continued until preconfluency at 37 °C. The medium was replaced with fresh serum-free medium containing 1 μM VP22-GFP. Cells were incubated for the indicated times or for 1 h, washed once with ice-cold PBS, and trypsinized for 15 min at 37 °C to eliminate non-internalized cell-surface protein. This was followed by centrifugation in 1.5-ml tubes, and the cells were washed three times with ice-cold PBS, lysed with PBS containing 0.5% Triton X-100, and disrupted by sonication. The cell lysate was centrifuged. The protein content of the supernatant was measured using a Bio-Rad protein assay kit with bovine serum albumin as the standard. Fluorescence intensity was measured with a Hitachi FL-2500 spectrofluorometer at a excitation wavelength of 488 nm and a emission wavelength of 511 nm. Replacement of 0.5% Triton X-100 with 0.1% SDS gave no appreciable difference in measurement, indicating that almost all internalized VP22-GFP is solubilized by 0.5% Triton X-100 treatment.

Low Temperature Treatment and ATP Depletion—For low temperature treatment, after being incubated at 4 °C for 1 h, the cells were further incubated in the presence of VP22-GFP for 1 h at 4 °C and subjected to trypsin digestion or fixation. For removal of cellular ATP, the cells were incubated with ATP depletion medium (glucose-free DMEM with 10 mM sodium azide and 6 mM 2-deoxy-D-glucose) containing 10% fetal calf serum for 1.5 h, followed by incubation in the presence of the indicated concentrations of VP22-GFP for 1 h in serum-free ATP depletion medium. Cellular protein uptake was visualized or measured as described above.

Quantification of Cell-surface VP22-GFP and Anti-heparan Sulfate Antibody Binding Signals—Cells were cultured in 12-well culture plates on a glass coverslip. Cells were washed twice with serum-free DMEM and incubated on ice for 1 h. After addition of the indicated concentrations of VP22-GFP or 2 μg/ml anti-heparan sulfate antibody in serum-free DMEM, cells were further incubated on ice for 1 h, washed twice with ice-cold PBS, fixed with 4% paraformaldehyde at room temperature for 15 min, and visualized by confocal microscopy. For anti-heparan sulfate antibody staining, the secondary antibody treatment was also carried out before paraformaldehyde fixation. A projection image was constructed using successive optical sections of 0.25 μm each. A region of interest was drawn around each cell, and the average intensity was calculated using the software that came with the confocal microscope.

Immunofluorescence—Cells were cultured in 12-well culture plates on a glass coverslip, incubated with protein at the specified concentrations in serum-free DMEM for the indicated times, washed twice with ice-cold PBS, and fixed with 4% paraformaldehyde at room temperature for 15 min. After being washed twice with ice-cold PBS, the cells were permeabilized with PBS containing 0.2% Triton X-100 and washed twice with ice-cold PBS. Nonspecific binding sites were blocked with PBS containing 5–10% goat whole serum (IBL Medical Products Co.) at room temperature for 30 min. Following incubation with the primary antibody (1:100–400 dilution) in PBS containing 1–5% goat whole serum for 1 h at room temperature or overnight at 4 °C, the cells were washed twice with PBS and treated with the secondary antibody (1:100–400 dilution) in PBS containing 1–5% goat whole serum for 1 h at room temperature or overnight at 4 °C. This was followed by two washes with PBS and visualization by confocal microscopy as described above.

RNA Interference (RNAi)—Two sets of human clathrin heavy chain small interfering RNA (siRNAs) were selected using siDirect (33): *CHC1* (clathrin heavy chain 1), GCUUCAGUACCCUGACUAUGG (passenger strand) and AUAGUCAGGGUACUGAAGCCA (guide strand); and *CHC2*, CCUGGUACGUCGAAAGGAUCC (passenger strand) and AUCCUUUCGACGUACCAGGUA (guide strand). Firefly luciferase siRNA was used as a control: CGUACGCGGAAUACUUCGAAA (passenger strand) and UCGAAGUAUUCCGCGUACGUG (guide strand). RNA oligonucleotides were synthesized by Proligo, and double-stranded siRNA was prepared as described previously (34). HeLa cells in 12-well plates were transfected three times at 24–36-h intervals with 50 nM siRNA. Firefly luciferase siRNA-treated and *CHC* siRNA-treated cells were trypsinized, mixed at a ratio of 1:1, and seeded in 12-well plates 20 h prior to observation of the effects of clathrin heavy chain depletion in the same field. DNA transfection was conducted with a third siRNA transfection.

DNA-mediated RNAi was also carried out to knock down the genes encoding RhoA, Cdc42, and Arf6. A firefly luciferase short hairpin RNA expression construct was used as a control. Details of vector construction will be described elsewhere.[6] HeLa cells in 12-well plates were transfected with a suitable construct, and transfectants were selected with puromycin (2 μg/ml) 24 h after transfection. Cells were analyzed 96 h after transfection.

Drug Treatment—Cells were washed twice with serum-free DMEM and incubated in serum-free DMEM containing a given drug at the indicated concentrations for 30 min except for *C. difficile* toxin B. Following protein addition to the medium, cells were incubated for 1 or 4 h. Protein uptake and cell-surface binding were visualized and measured as described above.

Triton X-100 Treatment—After being put on ice with 0.25 μM VP22-GFP, 2 μg/ml anti-CD59 antibody, or 1 μg/ml anti-

[6] K. Ui-Tei, K. Nishi, and K. Saigo, unpublished data.

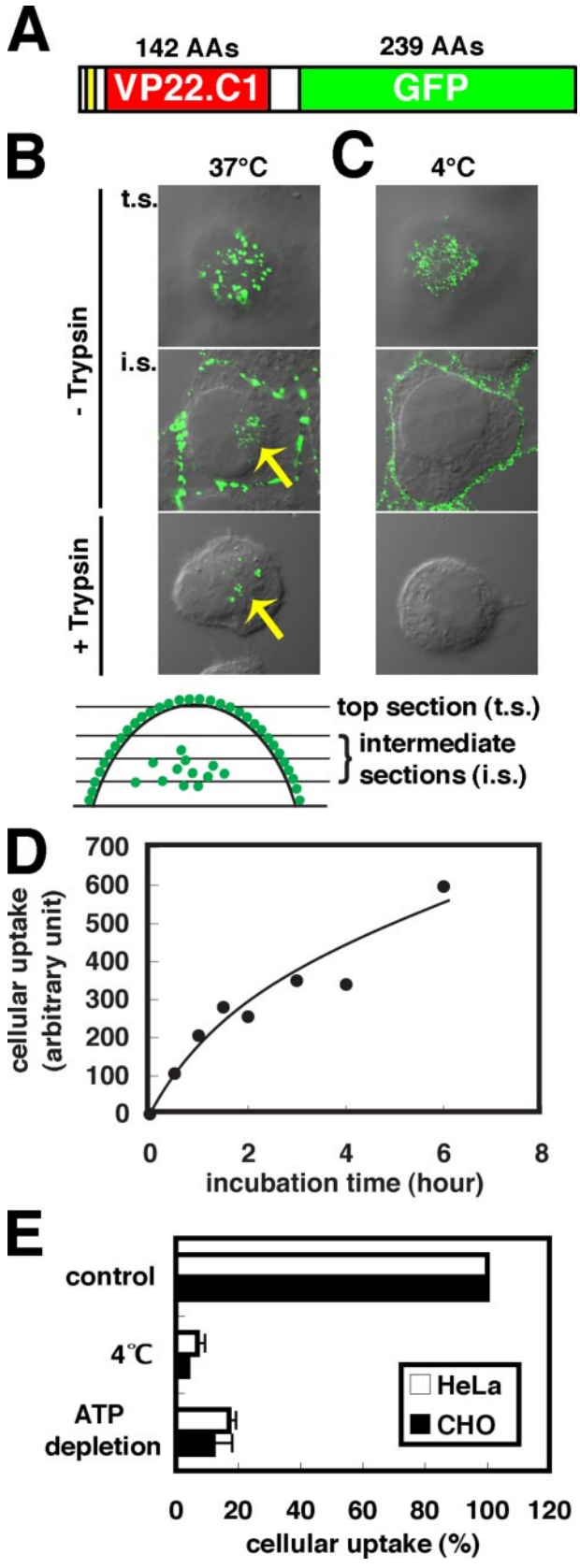

FIGURE 1. **Cellular VP22 uptake via endocytosis.** *A*, structure of VP22-GFP. The 6-amino acid histidine tag, VP22.C1, and GFP are shown in *yellow*, *red*, and *green*, respectively. *AAs*, amino acids. *B*, VP22-GFP signals in HeLa cells with (*lower panel*) or without (*upper* and *middle panels*) trypsin treatment. HeLa cells were exposed to 0.5 μM VP22-GFP at 37 °C for 1 h, fixed with paraformaldehyde, and observed under a confocal microscope. Cells were trypsinized before paraformaldehyde fixation. VP22-GFP signals (*green*) in the top and intermediate optical sections (see the lower margin) and a differential interference contrast image were merged. *Arrows* indicate internalized VP22-GFP signals. *C*, HeLa cells exposed to VP22-GFP at 4 °C. Note the absence of internalized VP22-GFP signals. *D*, time course of intracellular accumulation of VP22-GFP in HeLa cells at 37 °C. Cells were exposed to 1 μM VP22-GFP. The amount of intracellular VP22-GFP signals was measured spectrofluorometrically after trypsin treatment. Two measurements were averaged. *E*, effects of low temperature and ATP depletion on cellular uptake of VP22-GFP in HeLa and CHO-K1 cells. HeLa and CHO-K1 cells were exposed to 1 μM VP22-GFP at 4 °C or under ATP depletion conditions. Three independent spectrofluorometric measurements obtained after trypsin treatment were averaged. *Error bars* indicate S.D. The cellular uptake of VP22-GFP found in cells cultured under normal conditions at 37 °C is also shown (*control*).

transferrin receptor antibody on ice for 1 h, cells were washed twice with serum-free DMEM, stained with the secondary antibody for 1 h in serum-free DMEM, washed twice with ice-cold PBS, treated with 1% Triton X-100 in PBS for 7 min, and washed twice again with ice-cold PBS on ice. They were then fixed with 4% paraformaldehyde and visualized.

Cell Treatment with Glycosaminoglycan (GAG) Lyases—Enzymatic treatment with GAG lyases was carried out as reported previously (35). Briefly, preconfluent cells were washed once with PBS, followed by incubation with GAG lyases in PBS containing 0.1% bovine serum albumin, 0.2% gelatin, and 0.1% glucose for 2 h at 37 °C. Four washings with PBS or serum-free DMEM were carried out. Following addition of the indicated concentrations of VP22-GFP to the medium, cells were incubated for 1 h. VP22-GFP uptake and binding were visualized and measured as described above.

Real-time PCR—The total RNA from transfected cells was isolated using an RNeasy mini kit (Qiagen Inc.). The RNA was treated with RQ1 DNase (Promega Corp.), purified using the RNeasy mini kit, and reverse-transcribed using SuperScript III (Invitrogen). Before the PCR, a mixture of the synthesized cDNA and SYBR Green PCR Master Mix (Applied Biosystems) was incubated at 95 °C for 10 min. PCR was then carried out at 95 °C for 15 s and at 60 °C for 1 min for 40 cycles. All reactions were carried out in triplicate. The levels of PCR products were monitored with an ABI PRISM 7000 sequence detection system and analyzed with ABI PRISM 7000 SDS software (Applied Biosystems). For each sample, the amount of target mRNA was normalized using endogenous β-actin mRNA. The following primers were used: Arf6, 5′-ATCAATGACCGGGAGATGAG-3′ (forward) and 5′-AGGGCTGCACATACCAGTTC-3′ (reverse); Cdc42, 5′-CGATGGTGCTGTTGGTAAAA-3′ (forward) and 5′-TCCTCTTGCCCTGCAGTATC-3′ (reverse); RhoA, 5′-CGGTCTGGTCTTCAGCTACC-3′ (forward) and 5′-CCATCACCAACAATCACCAG-3′ reverse; and β-actin, 5′-CACACTGTGCCCATCTACGA-3′ (forward) and 5′-GCCATCTCTTGCTCGAAGTC-3′ (reverse).

RESULTS

Cellular Uptake of VP22-GFP Occurs through Endocytosis—To clarify the mechanism for the cellular uptake of VP22, VP22-GFP, a fusion protein between GFP and VP22.C1 (Fig. 1*A*), was prepared from *E. coli* cells and added to the culture medium with HeLa cells. GFP signal distribution was examined at 1 h of incubation at 37 °C using a confocal microscope (Fig. 1*B*). Significant VP22-GFP signals were observed not only on

the surface of the cells (Fig. 1*B*, *top section (t.s.)*) but also inside (*intermediate sections (i.s.)*). Fifteen minutes of trypsin treatment at 37 °C eliminated almost completely the cell-surface signals without affecting intracellular signal intensity (Fig. 1*B*, compare *middle* and *lower panels*). Cellular VP22-GFP uptake appeared to depend on the VP22 moiety because no intracellular GFP signal was detected upon elimination of the entire VP22.C1 moiety from the fusion protein (data not shown). Change in intracellular GFP signal intensity was examined spectrofluorometrically using trypsin-treated HeLa cells (Fig. 1*D*). The intracellular VP22-GFP signal increased gradually for >6 h.

Fig. 1*B* shows that the cytoplasmic distribution of VP22-GFP in HeLa cells is vesicular, supporting the notion that VP22-GFP is internalized through endocytosis (8). Endocytosis-dependent cellular internalization would not occur either at 4 °C or in the absence of ATP (7). As shown in Fig. 1 (*C* and *E*), no or hardly any intracellular accumulation of VP22-GFP could be detected in HeLa cells exposed to VP22-GFP at 4 °C. In contrast to cellular uptake, VP22-GFP adsorption onto the cell surface appeared to occur quite normally even at 4 °C. The cellular ATP pool becomes empty upon preincubation of cells with sodium azide and deoxyglucose (36). Only slight cellular uptake of VP22-GFP without significant reduction in surface signals was apparent in both ATP-depleted HeLa and CHO-K1 cells (Fig. 1*E*). VP22-GFP may thus be concluded to be internalized through endocytosis in HeLa and CHO-K1 cells.

Requirement of Heparan Sulfate for Cell-surface Binding and Cellular Uptake of VP22-GFP—Cellular internalization of TAT-PTD requires proteoglycans (11, 12). In the case of mammalian cell-surface GAGs, heparan sulfate and chondroitin sulfates A–C are the main components. We thus investigated whether GAGs are required for cell-surface adsorption and cellular uptake of VP22-GFP. After HeLa cells were treated with heparitinase or chondroitinase ABC, cell-surface adsorption and cellular uptake of VP22-GFP signals were assessed. Heparitinase digests heparan sulfate, whereas chondroitinase ABC digests chondroitin sulfates A–C but not heparan sulfate. Heparitinase treatment eliminated not only cell-surface VP22-GFP signals but cellularly internalized VP22-GFP signals as well (Fig. 2*A*). In contrast, virtually no reduction in VP22-GFP signals on either the surface of or inside cells could be detected by chondroitinase ABC treatment (Fig. 2*A*). GAGs were added to the culture medium, and only heparin (analog of heparan sulfate) addition was found to induce a significant reduction in intracellularly accumulated VP22-GFP signals (Fig. 2*B*). Thus, in HeLa cells, heparan sulfate (but not chondroitin sulfates) is required for the surface adsorption and intracellular accumulation of VP22-GFP.

pgsA-745 and pgsD-677 cells are mutant GAG strains of CHO-K1 cells (37, 38). pgsA-745 is deficient in xylosyltransferase, the key enzyme required for GAG attachment to core protein. Only 1% of GAGs expressed in wild-type cells have been reported to be expressed in pgsA-745 cells (37). In this study, very few if any heparan sulfate signals could be detected by anti-heparan sulfate antibody staining in both pgsA-745 and pgsD-677 cells (supplemental Fig. 1). pgsD-667 is deficient in *N*-acetylglucosaminyltransferase and glucuronyltransferase, both of which are essential for heparan sulfate polymerization. pgsD-667 cells have been shown not to produce heparan sulfate but instead 3–4 times as many chondroitin sulfate molecules as wild-type cells (38). Fig. 2*C* shows that cell-surface and internalized VP22-GFP signals underwent significant reduction in pgsA-745 and pgsD-667 cells; thus, as with HeLa cells, heparan sulfate (but not chondroitin sulfates) is required for VP22-GFP binding to the cell surface and internalization in CHO-K1 cells.

To further confirm the close relation between cell-surface VP22-GFP adsorption and heparan sulfate, we examined whether the distribution of VP22-GFP signals on the cell surface is in some way related to that of heparan sulfate signals (Fig. 2*D*). Anti-heparan sulfate antibody staining revealed that the heparan sulfate on the surface of HeLa cells was punctate. Nearly all punctate signals of heparan sulfate were found to co-localize with VP22-GFP signals that had distributed in a punctate fashion and vice versa (Fig. 2*D*). However, it should be noted that heparan sulfate signal intensity was not always proportional to VP22-GFP signal intensity, possibly suggesting involvement of other factors in cell-surface VP22-GFP adsorption.

Involvement of Basic Amino Acids in the VP22.C1 N-terminal Region in Cell-surface Adsorption and Intracellular Uptake of VP22-GFP—As with TAT-PTD, VP22.C1 is rich in basic amino acids (Fig. 2*E*) (23). Mutational analysis indicated that 8 basic amino acids in TAT-PTD are equally requisite for cellular uptake activity (39). To determine which basic amino acids of VP22.C1 are required for interactions between heparan sulfate and VP22-GFP, the basic amino acids of VP22.C1 were systematically replaced with alanine (neutral amino acid) or glutamic acid (acidic amino acid), and we examined spectrofluorometrically whether mutant VP22-GFP proteins were effectively incorporated into cells (Fig. 2*F*). The R164A and R164E mutant proteins were found to lose 90% of the intracellular incorporation activity of the wild-type protein, indicating the importance of arginine at position 164 for VP22-GFP internalization. At positions 174, 192, and 199, only glutamic acid substitutes exhibited significant reduction in internalization activity, suggesting that the absence of negative charges at these positions is required for effective intracellular uptake of VP22-GFP. Fig. 2*F* shows that most, if not all, other basic amino acids of VP22.C1, which are associated with moderate mutational effects, may also be involved in VP22-GFP internalization to some extent.

Reduction in VP22-GFP internalization activity appeared to be virtually proportional to that in cell-surface binding activity. Indeed, cell-surface VP22-GFP signals were almost completely abolished or significantly reduced in R164E, R164A, and R192E, three strong internalization-defective mutants, whereas cell-surface VP22-GFP signals in R192A and R207A, associated with moderate internalization defects, were moderately reduced (Fig. 2, compare *F* and *G*).

Requirement of Dynamin in Cellular Internalization of VP22-GFP—Dynamin is a GTPase that is essential for various endocytic pathways (10). Cellular expression of the GTPase-deficient, dominant-negative mutant of dynamin (dynamin-K44A) has no effect on macropinocytosis or certain lipid raft-mediated endocytic pathways, including that induced by Arf6-Q67L (32), but almost entirely blocks clathrin-mediated endocytosis and other lipid raft-mediated endocytic path-

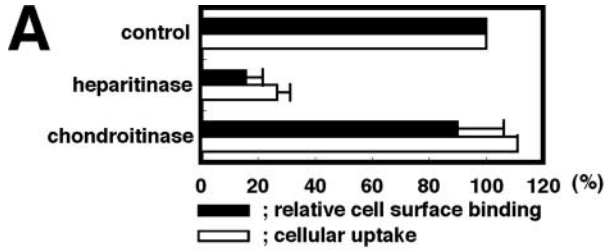

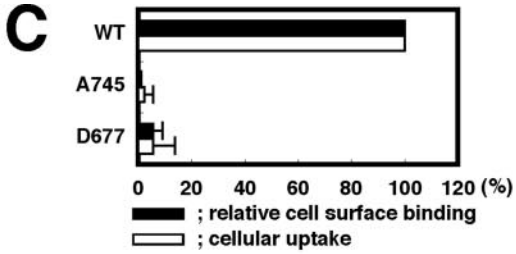

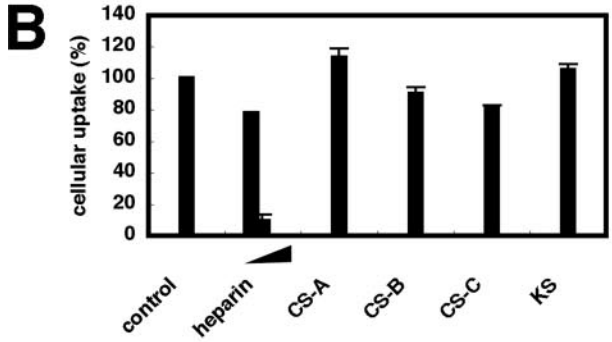

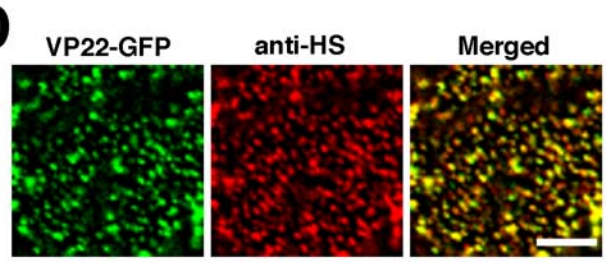

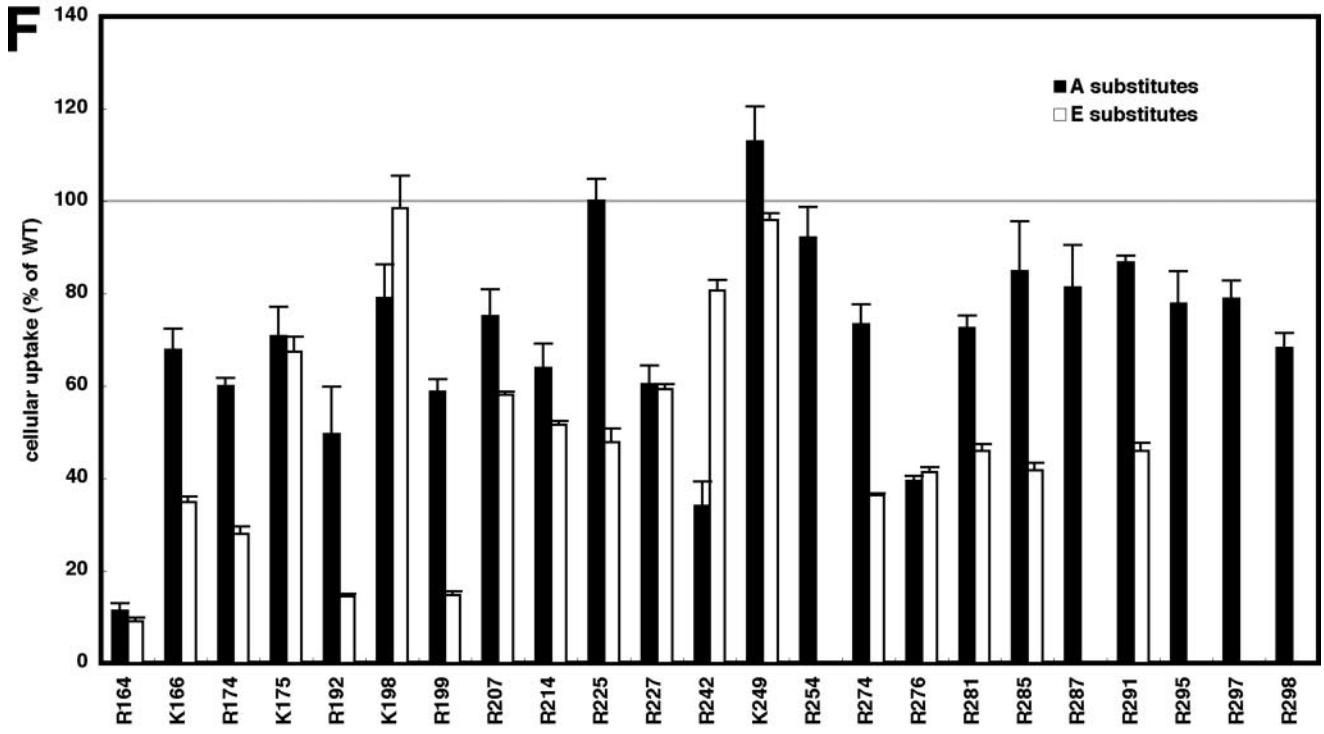

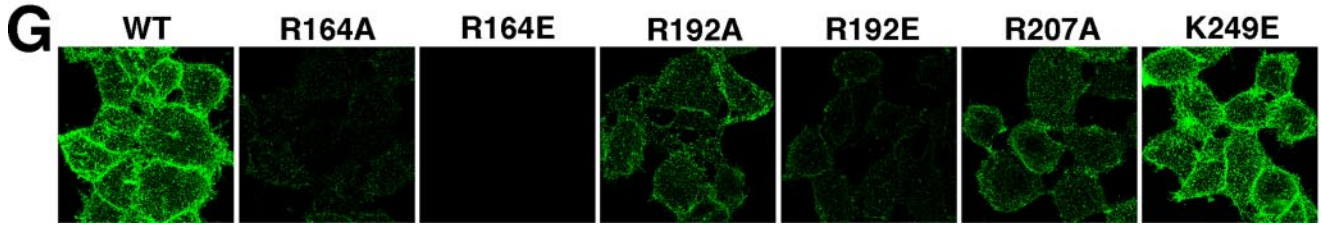

ways such as caveola-mediated endocytosis (10, 40–43). Using transferrin as a dynamin-dependent endocytosis marker, we examined VP22-GFP internalization in HeLa cells transfected with wild-type dynamin-2 or dynamin-2-K44A. Dynamin-overexpressing cells were identified by anti-HA antibody. Overexpression of wild-type dynamin-2 resulted in virtually no change in VP22-GFP and transferrin internalization (data not shown). In contrast the internalization of VP22-GFP and transferrin was noted to be significantly reduced in nearly 60 and 80% of cells overexpressing dynamin-2-K44A, respectively (Fig. 3, *A* and *C*). No apparent dynamin-2-K44A-dependent change in cell-surface heparan sulfate signals was observed (Fig. 3*B*). Dynamin-2 is thus essential for the normal cellular internalization of VP22-GFP, and also, VP22-GFP may not be internalized through macropinocytosis and lipid raft-mediated endocytosis induced by Arf6-Q67L but instead by clathrin-mediated endocytosis or dynamin-dependent lipid raft-mediated endocytosis, such as that mediated by caveolae. Note that heparan sulfate (Fig. 3*B*) as well as cell-surface VP22-GFP (Fig. 3*D*) signals were not affected by the absence of dynamin activity, indicating that dynamin is involved in cellular uptake, but not in VP22-GFP adsorption.

VP22-GFP Endocytosis Is Independent of Clathrin—By far, clathrin-mediated endocytosis has been best characterized and has been shown to be inhibited specifically by chlorpromazine (44). Cell treatment with chlorpromazine induces clathrin-coated pit misassembly at the plasma membrane, so clathrin-mediated endocytosis such as transferrin uptake is prevented to a significant degree in chlorpromazine-treated cells. To confirm any possible involvement of clathrin-mediated endocytosis in the cellular internalization of VP22, we examined the effects of chlorpromazine treatment on VP22-GFP internalization in HeLa cells (Fig. 4, *A* and *B*).

Chlorpromazine treatment (10 μg/ml, 30 min) significantly reduced transferrin internalization in 60% of the cells (Fig. 4*A*, *arrows*), whereas VP22-GFP internalization was actually enhanced in virtually all cells exhibiting a significant reduction in transferrin uptake (Fig. 4*A*). Clathrin-mediated endocytosis thus apparently is not involved in VP22-GFP internalization in HeLa cells.

For further clarification of the above, the *CHC* gene was knocked down using RNAi because clathrin-mediated endocytosis was reported previously to be severely inhibited in clathrin-depleted cells (45, 46). For observation of clathrin-depleted and non-depleted cells in the same field, a 1:1 mixture of *CHC1* siRNA-treated cells and firefly luciferase siRNA (control siRNA unrelated in sequence to the *CHC* gene)-treated cells was

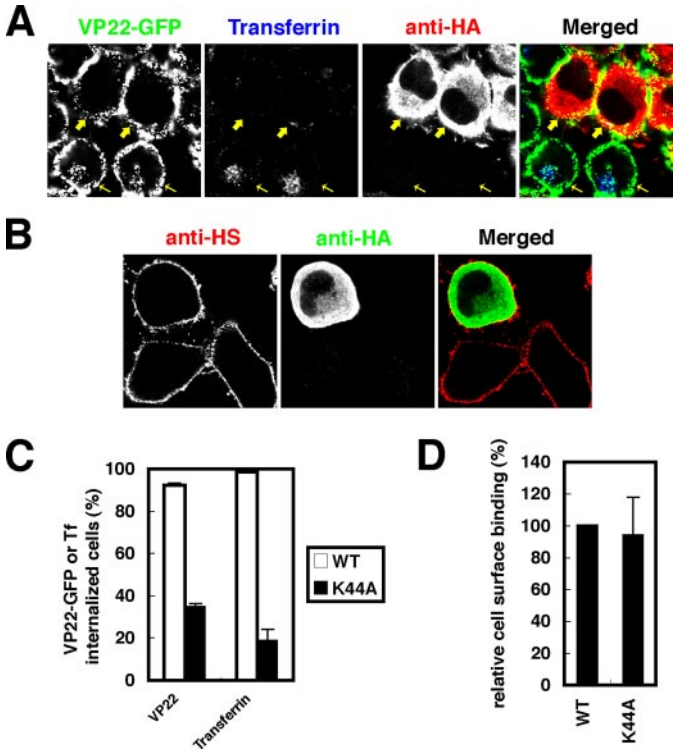

FIGURE 3. **Requirement of dynamin for VP22-GFP endocytosis.** *A*, HeLa cells transfected with pcDNA3-HA-dynamin-2a-K44A, an expression plasmid encoding an HA-tagged dominant-negative form of dynamin (K44A). Cells were exposed to VP22-GFP (0.5 μM) and Alexa Fluor 647-labeled transferrin (0.25 μM) 24 h after transfection. *Thick arrows* show anti-HA antibody-stained K44A-expressing cells, and *thin arrows* show normal cells exhibiting intracellular accumulation of VP22-GFP and transferrin signals but lacking dynamin activity. *B*, normal accumulation of heparan sulfate on the surface of cells lacking dynamin activity. Cell-surface heparan sulfate was detected by anti-heparan sulfate (*anti-HS*) antibody. Note that heparan sulfate signals were not reduced in cells expressing dynamin-K44A. *C*, proportion of cells associated with internalized signals of VP22-GFP or Alexa Fluor 647-labeled transferrin (*Tf*). Measurements from two independent experiments were averaged (each case, $n \geq 30$). *Error bars* indicate S.D. *D*, cell-surface VP22-GFP signals in K44A-expressing cells. HeLa cells transfected with pcDNA3-HA-dynamin-2a-WT or pcDNA3-HA-dynamin-2a-K44A were incubated for 1 h on ice with fresh serum-free medium containing 0.25 μM VP22-GFP. Surface signals were determined by confocal microscopy ($n \geq 33$). *Error bars* indicate S.D. *WT*, wild-type dynamin-2.

FIGURE 2. **Requirement of cell-surface heparan sulfate and VP22.C1 basic amino acids for cellular internalization of VP22-GFP.** *A*, effects of heparitinase or chondroitinase treatment on cell-surface binding and intracellular accumulation of VP22-GFP. HeLa cells were treated with 25 milliunits/ml heparitinase or chondroitinase ABC and exposed to 0.25 μM (cell-surface binding) or 1 μM (intracellular accumulation) VP22-GFP for 1 h. *Black bars*, cell-surface VP22-GFP signals measured using a confocal microscope ($n \geq 23$) (see "Experimental Procedures"); *white bars*, intracellular GFP signals measured spectrofluorometically after trypsin treatment. Three independent measurements were averaged. *Error bars* indicate S.D. *B*, inhibition of intracellular VP22-GFP accumulation by GAGs. Cells were exposed to 1 μM VP22-GFP in medium containing 1–25 μg/ml heparin (analog of heparan sulfate) and 25 μg/ml chondroitin sulfate (*CS*) A, B, or C or keratan sulfate (*KS*) for 1 h, and intracellular GFP signals were measured spectrofluorometically after trypsin treatment. Three independent measurements were averaged. *C*, relative cell-surface binding (*black bars*) and intracellular accumulation (*white bars*) of VP22-GFP in wild-type (*WT*) and mutant (pgsA-745 and pgsD-677) CHO-K1 cells. Cell-surface binding (0.5 μM VP22-GFP; $n \geq 34$) and intracellular accumulation (1 μM VP22-GFP; six measurements) of VP22-GFP signals were determined as described for *A*. *D*, co-localization of VP22-GFP and heparan sulfate signals on the HeLa cell surface. HeLa cells were incubated for 1 h on ice with fresh serum-free medium containing 0.25 μM VP22-GFP and 2 μg/ml anti-heparan sulfate (*anti-HS*) antibody. The secondary antibody treatment was carried out before paraformaldehyde fixation. A cell-surface section is shown. *Scale bar* = 5 μm. *E*, amino acid sequence of VP22.C1. Ser^{159} of VP22 corresponds to the N terminus of VP22.C1. Basic amino acids are shown in *red*. *F* and *G*, effects of the substitution of basic amino acids of VP22.C1 on intracellular accumulation (1 μM VP22-GFP; *F*) and cell-surface binding (0.25 μM VP22-GFP; *G*) of VP22-GFP. *Black bars*, intracellular accumulation in alanine-substituted mutants; *white bars*, intracellular accumulation in glutamic acid-substituted mutants. Intracellular accumulation of VP22-GFP signals was determined spectrofluorometrically after trypsinization. Three measurements were averaged. R254E, R287E, R295E, R297E, and R298E are not tested. Cell-surface signals were observed under a confocal microscope (projection figures; *G*). Note that cell-surface VP22-GFP signals were significantly reduced in R164A-, R164E-, and R192E-exposed cells. R192A and R207A gave moderately reduced signals, whereas K249E gave virtually no reduction in signal intensity.

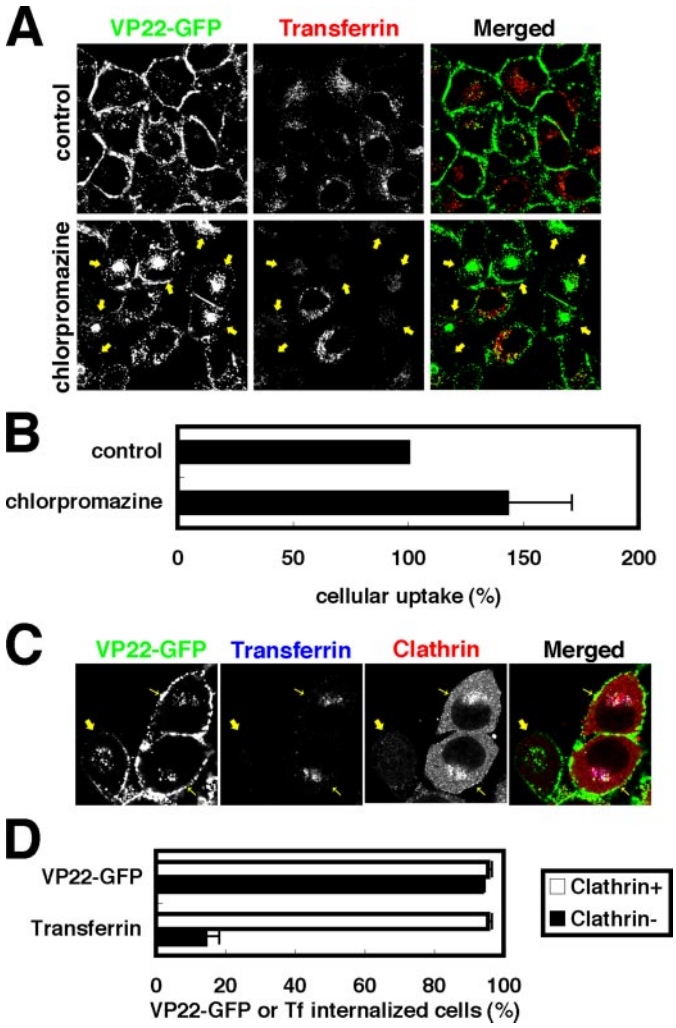

FIGURE 4. **Clathrin-independent cellular uptake of VP22-GFP.** *A*, stimulation of intracellular VP22-GFP accumulation by chlorpromazine treatment. *Lower panels*, HeLa cells treated with 10 μg/ml chlorpromazine for 30 min were exposed to 0.5 μM VP22-GFP and 0.25 μM Alexa Fluor 647-labeled transferrin at 37 °C for 1 h. *Arrows* show cells with reduced transferrin uptake. In these cells, intracellular VP22-GFP signals significantly increased, indicating that clathrin is not involved in cellular uptake of VP22-GFP. *B*, quantitative data for chlorpromazine-dependent intracellular VP22-GFP signal accumulation. After chlorpromazine treatment, cells were exposed to 1 μM VP22-GFP for 1 h. Measurements from three experiments were averaged. *Error bars* indicate S.D. *C*, effect of *CHC1* RNAi. RNAi for the clathrin heavy chain was carried out using *CHC1* siRNA. *Thick arrows* show clathrin-negative cells in which internalized transferrin (but not VP22-GFP) signals were abolished, and *thin arrows* show wild-type cells with clathrin production. *D*, proportion of cells associated with internalized signals of VP22-GFP or Alexa Fluor 647-labeled transferrin (*Tf*) in anti-clathrin antibody-positive (*Clathrin*+) or -negative (*Clathrin*−) cells. Measurements from two independent experiments were averaged (each case, $n \geq 50$). *Errors bars* indicate S.D.

plated. In clathrin-negative cells, transferrin uptake was almost completely inhibited, whereas VP22-GFP uptake was essentially the same as that in clathrin-positive normal cells (Fig. 4, *C* and *D*); but unlike the case of chlorpromazine treatment, no apparent enhancement of VP22-GFP uptake could be detected (Fig. 4, compare *A* and *C*). Essentially the same was noted with RNAi using a different *CHC* siRNA (*CHC2*) (data not shown), indicating that the siRNA-induced change is not due to the off-target effects (47) but instead to the knockdown of clathrin gene activity. The cellular uptake of VP22-GFP may thus be concluded to be independent of clathrin-mediated endocytosis.

Lipid Raft Dependence of Cellular Uptake of VP22-GFP—Dynamin-2 is required for certain lipid raft-mediated endocytic pathways such as caveola-mediated endocytosis. We thus examined whether VP22-GFP uptake is dependent on lipid raft-mediated endocytosis. Lipid rafts are detergent (Triton X-100)-resistant domains rich in cholesterol and sphingolipids (48), and CD59 serves as a marker for a subgroup of lipid rafts (32). Cell-surface signals of not only CD59 but also VP22-GFP were found to be resistant to Triton X-100 treatment (Fig. 5*A*), but virtually all transferrin receptor signals, internalized in a lipid raft-independent manner, were completely eliminated subsequent to Triton X-100 treatment (Fig. 5*A*). Double staining showed that cell-surface VP22-GFP signals partially overlapped (if at all) CD59 signals in Triton X-100-treated HeLa cells (Fig. 5*B*), suggesting that VP22 may be internalized by endocytosis in a different way compared with CD59. Consistent with this, most intracellular VP22-GFP signals were found not to be co-localized with internalized CD59 signals at early stages (Fig. 5*C* and supplemental Fig. 2*A*), although at late stages in particular, in most cells expressing Arf6-Q67L, VP22-GFP signals were co-localized with large CD59-positive Arf6-Q67L-induced vesicles (Fig. 5*D*) (32). Cell-surface heparan sulfate-binding proteins such as lipoprotein lipase were shown previously to be resistant to Triton X-100 treatment (49), indicating the presence of heparan sulfate on the surface of Triton X-100-treated cells.

MβCD disrupts lipid rafts (50). Genistein is a tyrosine kinase inhibitor that prevents lipid raft-mediated endocytosis such as caveola-dependent endocytosis (50–52). Consistent with the notion that VP22-GFP is internalized through lipid raft-mediated endocytosis, intracellular VP22-GFP signals in HeLa cells were significantly reduced subsequent to MβCD (Fig. 5*E*) or genistein (Fig. 5*F*) treatment. MβCD treatment did not change the intensity of cell-surface heparan sulfate signals, whereas a considerable heparan sulfate signal was abolished by genistein treatment (Fig. 5*H*), suggesting that genistein may prevent VP22-GFP internalization via reduction in cell-surface heparan sulfate.

The actin cytoskeleton is required for lipid raft-mediated endocytosis such as that mediated by caveolae (52). Upon treatment of HeLa cells with cytochalasin D, an actin-depolymerizing reagent, actin filament disruption occurred, with consequent large membrane bleb (Fig. 5*G*) or protrusion (53) formation on the cell surface. Virtually all cell-surface VP22-GFP signals appeared to be co-localized with membrane blebs induced by cytochalasin D (Fig. 5*G*). A similar phenomenon has been reported to occur in the case of the *Helicobacter pylori* vaculating cytotoxin VacA (53). In cytochalasin D-treated cells manifesting these membrane blebs, the cellular uptake of VP22-GFP was significantly reduced (Fig. 5, *F* and *G*) without reduction in cell-surface heparan sulfate signals (Fig. 5*H*). It may thus follow that VP22-GFP is internalized via lipid raft-mediated endocytosis.

Caveolae Are Not Involved in VP22-GFP Internalization—To determine whether caveolae are involved in VP22-GFP internalization, we examined the possible requirement of caveolae for the cellular internalization of VP22-GFP. In cells other than those derived from muscle, caveolin-1 is a major structural

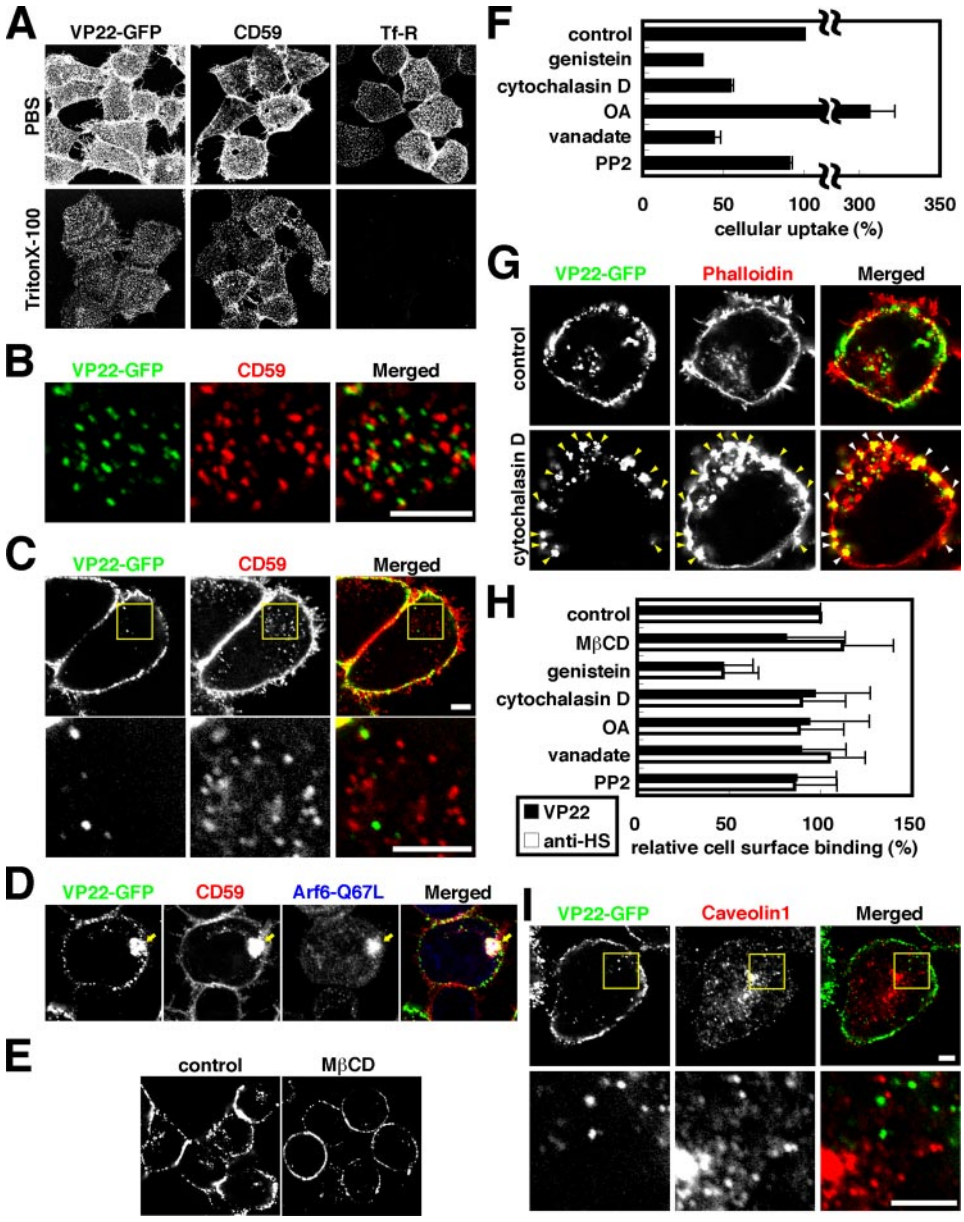

FIGURE 5. **Requirement of lipid rafts for VP22 endocytosis.** *A*, HeLa cells exposed to VP22-GFP, anti-CD59 antibody, or anti-transferrin receptor (*Tf-R*) antibody were treated with Triton X-100. Projection images of successive 0.25-μm optical sections are shown. The cell-surface signals of VP22-GFP were resistant to Triton X-100 treatment, whereas those of the transferrin receptor were completely eliminated. *PBS* indicates the control. *B–D*, relationship between cell-surface (*B*) and intracellular (*C* and *D*) signals of VP22-GFP and CD59. *B*, after HeLa cells exposed to 0.25 μM VP22-GFP were treated with Triton X-100, cells were stained with anti-CD59 antibody. A cell-surface section is shown. *Scale bar* = 5 μm. *C*, cells were exposed to 0.5 μM VP22-GFP and 2 μg/ml anti-CD59 antibody on ice for 1 h, washed, incubated at 37 °C for 15 min, fixed with 4% paraformaldehyde, and stained with secondary antibody. In the *Merged panels*, VP22-GFP and CD59 signals are shown in *green* and *red*, respectively. The *boxed regions* in the *upper panels* are enlarged in the *lower panels*. *Scale bars* = 5 μm. Cell-surface signals and early (5–15 min) intracellular signals of VP22-GFP overlapped only partially with the corresponding signals of CD59. *D*, HeLa cells transfected with the pXS-HA-Arf6-Q67L plasmid were allowed to internalize VP22-GFP and anti-CD59 antibody at 37 °C for 60 min, fixed with 4% paraformaldehyde, and stained with anti-HA antibody. At a late stage (60 min) in Arf6-Q67L-expressing cells, VP22-GFP signals were almost completely co-localized with CD59 signals. *Arrows* show Arf6-Q67L-induced vacuolar structures. *E*, HeLa cells treated with 10 mM MβCD for 30 min were exposed to 0.5 μM VP22-GFP at 37 °C for 1 h and fixed with 4% paraformaldehyde. MβCD appeared to prevent VP22-GFP signals from intracellularly accumulating. MβCD-treated cells exhibited a considerable instability to trypsinization. *F*, shown are the effects of genistein, cytochalasin D, okadaic acid (*OA*), vanadate, and PP2 on intracellular VP22-GFP accumulation. HeLa cells were treated with 100 μg/ml genistein, 10 μM cytochalasin D, 1 μM okadaic acid, 1 mM vanadate, or 10 μM PP2 for 30 min and then cells exposed to 1 μM VP22-GFP at 37 °C for 1 h. Measurements from three to six experiments were averaged. *Error bars* indicate S.D. *G*, shown are the morphological changes induced by cytochalasin D treatment. HeLa cells treated with 10 μM cytochalasin D for 30 min were exposed to VP22-GFP (0.5 μM). VP22-GFP and phalloidin-labeled rhodamine signals are shown in *green* and *red*, respectively. *Arrowheads* indicate VP22-GFP-accumulated membrane blebs. *H*, shown is the drug treatment dependence on cell-surface heparan sulfate and VP22-GFP signals. Except for genistein treatment, no appreciable reduction in cell-surface heparan sulfate signals was detected microscopically. In the case of genistein treatment, ~60% of the cell-surface heparan sulfate signals were lost. Anti-heparan sulfate (*anti-HS*) antibody and cell-surface VP22-GFP signals were determined by confocal microscopy ($n \geq 31$). *Error bars* indicate S.D. *I*, shown is the relationship between VP22-GFP and caveolin-1 signals. Cells were exposed to 0.5 μM VP22-GFP on ice for 1 h, washed, incubated at 37 °C for 15 min, fixed with 4% paraformaldehyde, and stained with anti-caveolin-1 antibody. In the *Merged panels*, VP22-GFP and caveolin-1 signals are shown in *green* and *red*, respectively. The *boxed regions* in the *upper panels* are enlarged in the *lower panels*. No overlap between intracellular VP22-GFP and caveolin-1 signals was observed. *Scale bars* = 5 μm.

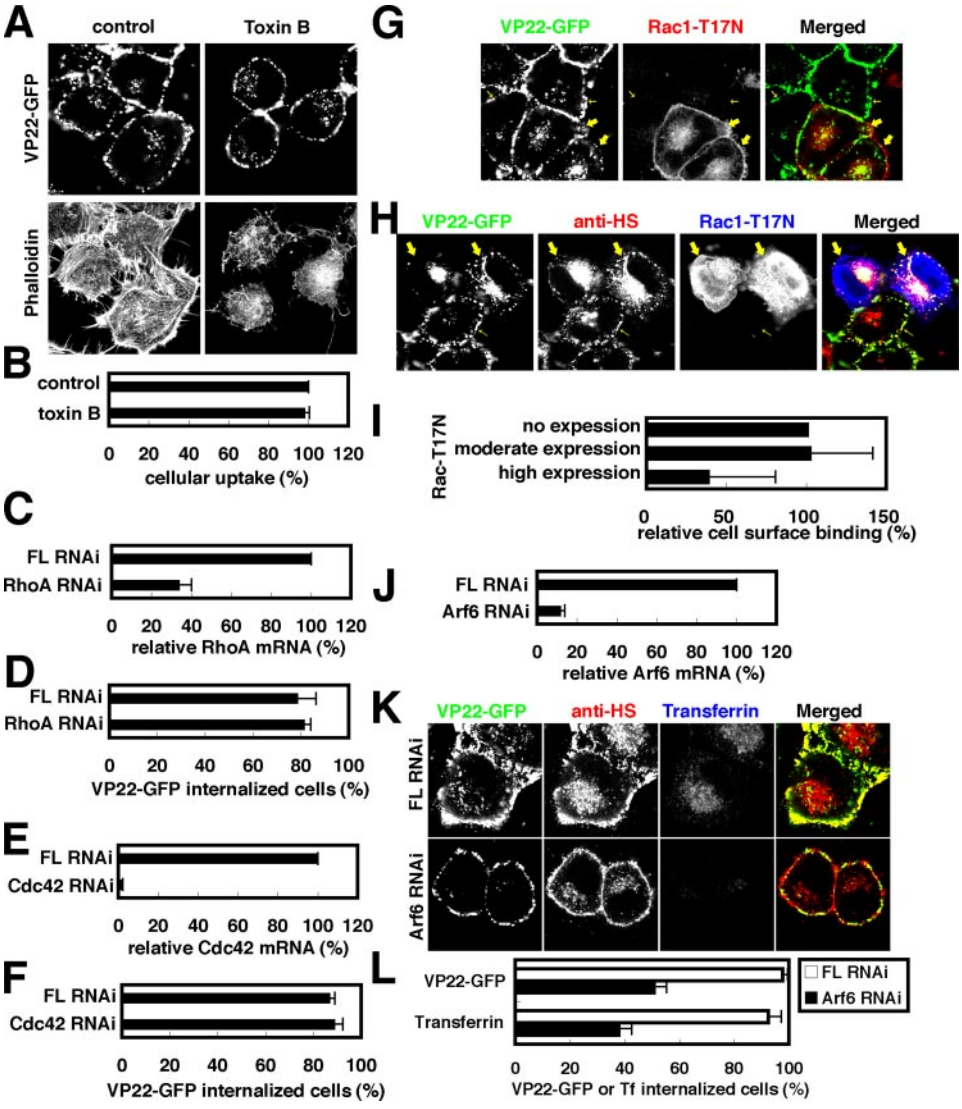

FIGURE 6. **Possible roles of small GTPases in VP22-GFP internalization.** *A*, effect of toxin B on intracellular VP22 accumulation. HeLa cells treated with 0.5 μg/ml *C. difficile* toxin B at 37 °C for 4 h were exposed to 0.5 μM VP22-GFP at 37 °C for 1 h, fixed with 4% paraformaldehyde, and stained with phalloidin-labeled rhodamine. Phalloidin images are those for the bottom of the cells. *B*, quantitative analysis of toxin B effects. Little effect of toxin B on intracellular VP22 accumulation was observed. Three spectrofluorometric measurements were averaged. *Error bars* indicate S.D. *C* and *D*, effect of RhoA RNAi on intracellular VP22 accumulation. RhoA mRNA was significantly reduced (*C*), but no reduction in VP22 internalization was evident (*D*). Firefly luciferase (*FL*) RNAi served as the control. *E* and *F*, effect of Cdc42 RNAi on VP22 uptake. Cdc42 mRNA was almost completely eliminated (*E*), but little reduction in VP22 internalization was detected (*F*). *G–I*, effect of overexpression of Rac1-T17N, a dominant-negative form of Rac1. HeLa cells were transfected with pRK5-myc-Rac1-T17N. Twenty-four hours after transfection, cells were exposed to 0.5 μM VP22-GFP at 37 °C for 1 h, fixed with 4% paraformaldehyde, and stained with anti-Myc antibody. In *H*, cells were also stained with anti-heparan sulfate (*anti-HS*) antibody. Cells moderately and highly expressing Rac1-T17N are shown in *G* and *H*, respectively. *Thick arrows* show Rac1-T17N expressing cells, and *thin arrows* show cells lacking Rac1-T17N expression. Strong internalized signals of VP22-GFP and heparan sulfate were found in cells expressing a high level of Rac1-T17N. In these cells, cell-surface signals of VP22 and heparan sulfate were occasionally reduced. Quantitative data are shown in *I*. Cell-surface VP22-GFP signals were measured by confocal microscopy ($n \geq 71$). *J–L*, effect of Arf6 RNAi on intracellular VP22 and transferrin accumulation. Not only Arf6 mRNA (*J*) but also VP22 and transferrin internalization (*K* and *L*) were significantly eliminated subsequent to Arf6 RNAi. HeLa cells transfected with pSUPER-retro-puro-FL or pSUPER-retro-puro-Arf6 were exposed to 0.5 μM VP22-GFP and 0.25 μM Alexa Fluor 647-labeled transferrin, fixed with 2% paraformaldehyde, and stained with anti-heparan sulfate antibody. Cell-surface heparan sulfate signals appeared to be reduced to some extent in Arf6 knockdown cells.

component of caveolae, and consequently, ligands of caveola-mediated endocytosis enter caveolin-1-positive subcellular compartments (54, 55). To determine the subcellular distribution of VP22-GFP at early stages of cellular uptake, HeLa cells were incubated in the presence of VP22-GFP at 0 °C, washed, and incubated again at 37 °C for 15 min. Hardly any internalized VP22-GFP signals were localized with caveolin-1 signals (Fig. 5*I* and supplemental Fig. 2*B*), indicating that VP22-GFP is internalized independently of caveolae.

Caveola-mediated endocytosis is enhanced by okadaic acid, an inhibitor of several protein serine/threonine phosphatases, and vanadate, an inhibitor specific for tyrosine phosphatases (56). In HeLa cells, okadaic acid treatment enhanced cellular VP22-GFP uptake, but there was no apparent okadaic acid-dependent stimulation of VP22-GFP internalization in CHO-K1 cells (data not shown). Vanadate brought about no enhancement of VP22-GFP internalization but instead significantly reduced the uptake of VP22-GFP in either cell type (Fig. 5*F*). PP2 is an Src kinase-specific inhibitor and prevents caveola-mediated endocytosis (57). Fig. 5*F* shows that VP22-GFP internalization was completely resistant to PP2 treatment. No appreciable change in cell-surface heparan sulfate signals was found upon treatment with okadaic acid, vanadate, or PP2 (Fig. 5*H*). It follows conclusively from these findings that VP22-GFP internalization takes place through a caveola-independent type of lipid raft-mediated endocytosis.

Rho Family GTPases Are Not Required for Cellular Internalization of VP22-GFP—Small GTPases are grouped into five families, Ras, Rho, Rab, Arf, and Ran (58), some of which have been shown recently to be differentially involved in lipid raft-mediated endocytosis (10). Rho family GTPases include Cdc42, RhoA, and Rac1. RhoA and Rac1 are required for lipid raft-mediated endocytosis of interleukin-2 receptors (42), whereas Cdc42 is involved in that of glycosylphosphatidylinositol-anchored proteins (59). *C. difficile* toxin B specifically inactivates Rho family GTPases through monoglucosylation (60). To examine the possible involvement of Rho family GTPases in VP22-GFP internalization, HeLa cells were treated with 0.2–1 μg/ml toxin B, which resulted in typical morphological changes such as cell rounding and actin filament disruption. As shown

in Fig. 6 (*A* and *B*), toxin B treatment brought about significant changes in cell morphology and the actin cytoskeleton, but there was no appreciable reduction in internalized VP22-GFP signals in toxin B-treated cells, suggesting that Rho family GTPases are not involved in VP22-GFP internalization.

To further confirm this point, HeLa cells were subjected to DNA-mediated RNAi to knock down the genes encoding RhoA (Fig. 6, *C* and *D*) and Cdc42 (*E* and *F*). Rac1 activity was depleted by overexpressing a dominant-negative form of Rac1 (Rac1-T17N) (Fig. 6, *G–I*). RhoA and Cdc42 mRNAs were significantly eliminated by RNAi (Fig. 6, *C* and *E*), but no appreciable reduction in VP22-GFP internalization was detected (*D* and *F*). Rac1-T17N expression levels varied depending on the cells. About 70% of the cells expressed Rac1-T17N moderately and exhibited a slight increment in internalized VP22-GFP signals without any substantial loss of surface signals (Fig. 6*G*), supporting the notion that Rac1 is not essential for cellular VP22 internalization. In the remaining cells, not only cell-surface VP22-GFP signals but also cell-surface heparan sulfate signals were frequently observed to be considerably reduced, and instead, the cellular internalized signals of both VP22-GFP and heparan sulfate were increased (Fig. 6, *H* and *I*). We interpreted these findings as suggesting that high levels of Rac1-T17N expression might result in rapid cellular uptake of cell-surface complexes of heparan sulfate and VP22-GFP. We thus concluded that Rho family small GTPases are not essential for normal VP22-GFP internalization.

Arf6 is a member of the Arf family and is essential for certain lipid raft- or clathrin-mediated endocytosis (10, 61). To show Arf6 involvement in VP22-GFP internalization, short hairpin RNA specific for *arf6* was used to knock down *arf6* activity. In Fig. 6 (*K* and *L*), internalized VP22-GFP and transferrin signals were significantly reduced upon elimination of *arf6* activity by RNAi (Fig. 6*J*). Arf6 is thus assumed to be involved in cellular VP22-GFP internalization. Because cell-surface heparan sulfate signals were occasionally observed to be reduced moderately in Arf6 knockdown cells (Fig. 6*K*), Arf6 may be partly involved in recruitment of heparan sulfate to the cell surface. Transferrin internalization was inhibited by *arf6* depletion in the HeLa cells used here; this is inconsistent with previous findings for human embryonic kidney 293 and HeLa cells (61, 62) and could suggest differences in cell lines.

Co-localization of VP22-GFP and Transferrin in Early Endosomes—To determine the subcellular localization of internalized VP22-GFP signals, clarification was sought as to whether VP22-GFP signals are co-localized with cell compartment markers. HeLa cells were exposed to VP22-GFP at 0 °C, and VP22-GFP that was not bound to cells was removed by washing at 0 °C. VP22-GFP internalization was then examined by shifting cells to 37 °C. Most, if not all, cytoplasmic VP22-GFP signals at 15 min of internalization were found to have co-localized with EEA1, an early endosomal marker (Fig. 7*A* and supplemental Fig. 3*A*), but not with LAMP1, a lysosomal marker (Fig. 7*B* and supplemental Fig. 3*B*), or GM130, a Golgi marker (Fig. 7*C* and supplemental Fig. 3*C*). Internalized VP22-GFP signals are thus initially incorporated into early endosomes marked with EEA1.

At 60 min of internalization, a considerable number of VP22-GFP molecules appeared to have moved from early endosomes to lysosomes for degradation. Overlapping between VP22-GFP and EEA1 signals at 60 min became less prominent than that at 15 min (Fig. 7, *E* and *I*; and supplemental Fig. 3*A*); instead, some VP22-GFP signals appeared to overlap LAMP1 signals (Fig. 7, *F* and *I*; and supplemental Fig. 3*B*), suggesting that VP22-GFP is partially transferred to the lysosome at later stages. There was no overlap between VP22-GFP and GM130 signals (Fig. 7, *G* and *I*; and supplemental Fig. 3*C*).

Transferrin (internalized through clathrin-mediated endocytosis) accumulates in early endosomes initially and in recycling endosomes at later stages (63). We thus compared the subcellular location of VP22-GFP and transferrin signals at 15 and 60 min (Fig. 7, *D*, *H*, and *I*; and supplemental Figs. 2*C* and 3*D*). Nearly all VP22-GFP signals were found to have co-localized with transferrin signals at both 15 and 60 min of internalization. Thus, the above findings indicate that VP22-GFP and transferrin, internalized with different mechanisms, accumulate in the same early endosomes immediately following internalization and in recycling endosomes at later stages.

To further confirm the close relationship between internalized VP22-GFP and transferrin in early endosomes, a constitutively active Rab5 mutant (Rab5-Q79L) known to stimulate early endosomal fusion to form ring-shaped large endosomes (64) was used. In HeLa cells overexpressing wild-type *rab5*, a gene encoding wild-type Rab5 tagged with Myc, the cellular distribution of VP22-GFP and transferrin was virtually the same as that in non-transfected HeLa cells (data not shown). But in HeLa cells overexpressing Myc-tagged Rab5-Q79L, VP22-GFP and transferrin were co-localized with ring-shaped endosomes, as visualized with anti-Myc antibody (Fig. 7*J* and supplemental Fig. 2*D*). To rule out the possibility that VP22-GFP enters Rab5-Q79L-positive structures via clathrin-mediated endocytosis, the clathrin heavy chain was abolished by RNAi (Fig. 7*K*). In clathrin-depleted cells, VP22-GFP entered ring-shaped endosomes, and this internalization was inhibited by genistein, an inhibitor of lipid raft-mediated endocytosis (data not shown). Rab5 and VP22-GFP rings and VP22-GFP and clathrin rings can be seen to differ slightly in position in Fig. 7*K*, thus possibly reflecting pathway-dependent substructures of early endosomes.

Stabilization of Internalized VP22-GFP Signals in Chloroquine-treated Cells—The biological activity of TAT-Cre has been shown to be significantly increased by chloroquine treatment (13), possibly suggesting that chloroquine enhances endosomal release of these proteins. We thus examined whether chloroquine treatment induces cytoplasmic non-vesicular VP22-GFP signals in HeLa and CHO-K1 cells. Cell were treated with 50 μM chloroquine, and possible changes in intracellular VP22-GFP signals were examined spectrofluorometrically and microscopically (Fig. 7, *L* and *M*). In contrast to our expectations, no apparent increase in cytoplasmic non-vesicular VP22-GFP signals was detected even after long chloroquine treatment. Chloroquine treatment instead significantly increased intracellular vesicular VP22-GFP signals in both cell lines. We interpret these

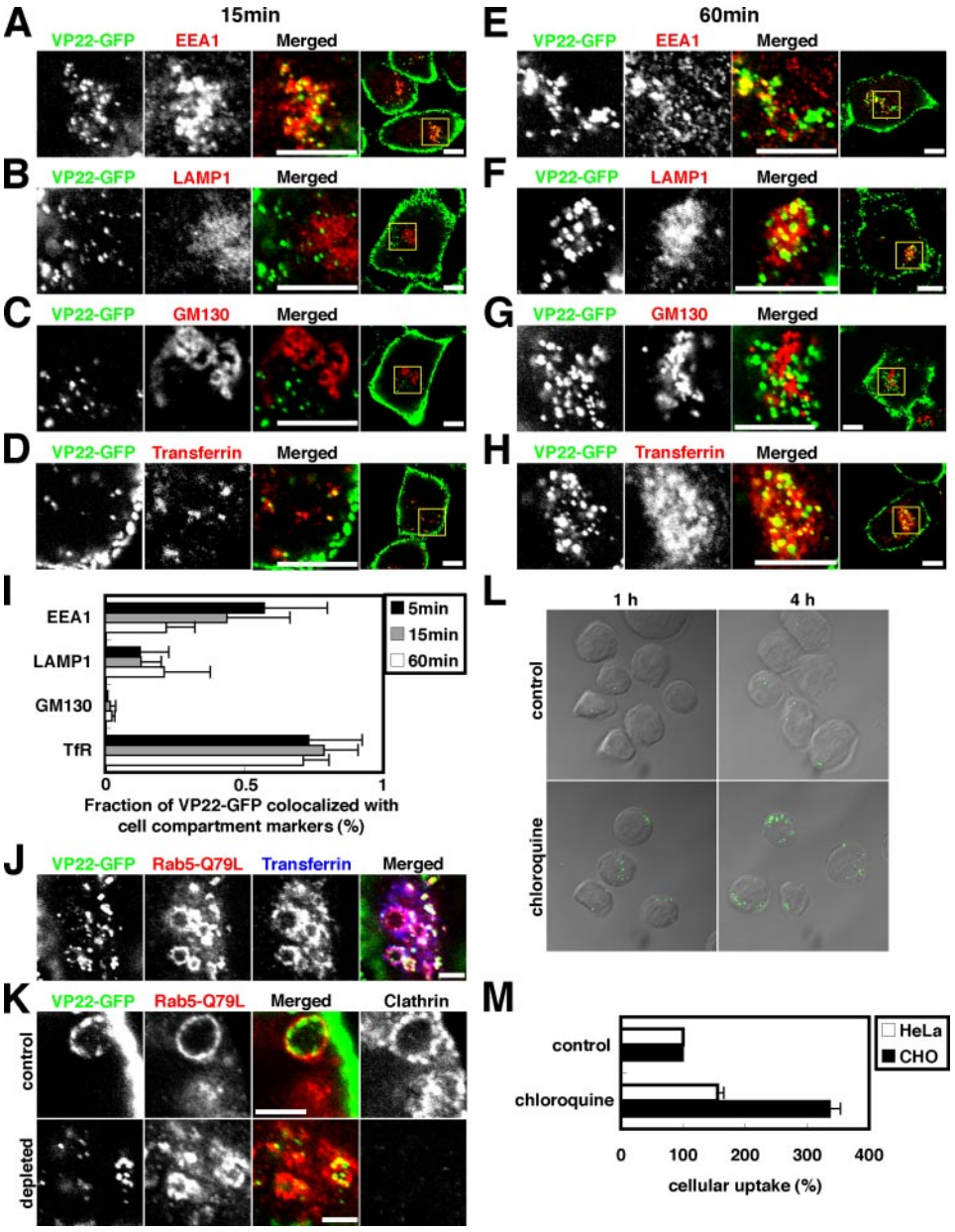

FIGURE 7. **Incorporation of internalized VP22 signals into early endosomes.** *A–H*, HeLa cells were exposed to 0.5 μM VP22-GFP and 0.25 μM Alexa Fluor 647-labeled transferrin at 0 °C; incubated for 15 min (*A–D*) or 60 min (*E–H*) at 37 °C; fixed with 4% paraformaldehyde; and stained with anti-EEA1 (*A* and *E*), anti-LAMP1 (*B* and *F*), and anti-GM130 (*C* and *G*) antibodies. Alexa Fluor 647-labeled transferrin signals are shown in *D* and *H*. In the *Merged panels*, VP22-GFP is shown in *green*, whereas EEA1, LAMP1, GM130, and transferrin are shown in *red*. The *boxed regions* in the *last panels* are enlarged in the *first three panels*. *Scale bars* = 10 μm. *I*, shown is the time course of the fraction of intracellular VP22-GFP co-localized with cell compartment markers. HeLa cells were exposed to 0.5 μM VP22-GFP at 0 °C and then incubated for 5, 15, or 60 min at 37 °C. After trypsin treatment at 37 °C for 5 min, cells were stained with anti-EEA1, anti-LAMP1, anti-GM130, and anti-transferrin receptor (*TfR*) antibodies and visualized by confocal microscopy. Co-localization was determined using the software that came with the confocal microscope (n = 12). *Error bars* indicate S.D. *J*, HeLa cells transfected with pcDNA3-myc-Rab5-Q79L, a plasmid encoding Myc-tagged Rab5-Q79L, were exposed to 0.5 μM VP22-GFP and 0.25 μM Alexa Fluor 647-labeled transferrin at 37 °C for 1 h; fixed with 4% paraformaldehyde; and stained with anti-Myc antibody. In the *Merged panel*, VP22-GFP, Myc-Rab5-Q67L, and transferrin are shown in *green*, *red*, and *blue*, respectively. *Scale bar* = 10 μm. *K*, HeLa cells transfected with *CHC1* siRNA and plasmids expressing Myc-Rab5-Q79L were incubated at 37 °C for 1 h with fresh serum-free medium containing 0.5 μM VP22-GFP, fixed with 4% paraformaldehyde, stained with anti-clathrin and anti-Myc antibodies. In the *Merged panels*, VP22-GFP and Rab5-Q79L are shown in *green* and *red*, respectively. *Scale bars* = 5 μm. *L* and *M*, the effects of chloroquine treatment on intracellular accumulation of VP22-GFP are shown. In *L*, CHO-K1 cells treated with 50 μM chloroquine for 30 min were exposed to VP22-GFP (1 μM), incubated for 1 or 4 h, and treated with trypsin. VP22-GFP signals (*green*) and a differential interference contrast image were merged. In *M*, HeLa and CHO-K1 cells treated with 50 μM chloroquine for 30 min were exposed to VP22-GFP (1 μM) and incubated for 1 h, and intracellular accumulation of VP22-GFP signals was determined spectrofluorometrically. Three independent measurements were averaged. *Error bars* indicate S.D.

results as suggesting that the predicted endosome-cytoplasm transfer of VP22-GFP may occur in a mechanism different from that of TAT-Cre.

DISCUSSION

In this work, we have shown that cell-surface binding and cellular internalization of VP22 require interactions between cell-surface heparan sulfate and basic amino acids in the N-terminal region of VP22.C1 (C-terminal half of VP22), which includes Arg-164, and that VP22 is internalized through a lipid raft-mediated endocytic pathway independent of clathrin, caveolae, and Rho family GTPases but dependent on dynamin and Arf6. We have also shown that internalized VP22 initially enters early endosomes and then moves to lysosomes and possibly recycling endosomes. Cellular uptake of VP22 appears to be unrelated to lipid raft-mediated endocytosis induced in Arf6-Q67L-expressing cells (32).

Differences in Cell-surface Adsorption between VP22-GFP and TAT-PTD—Fig. 2 shows that VP22-GFP bound to the cell surface mainly via heparan sulfate. The contribution of chondroitin sulfate to this binding is apparently quite small, if at all, because virtually no adsorption of VP22-GFP signals could be detected in pgsD-677, a CHO-K1 cell line capable of producing 3–4 times as many chondroitin sulfate molecules as wild-type cells without production of heparan sulfate. The intensity of internalized mutant VP22 signals was basically in proportion to that of signals adsorbed on the cell surface (Fig. 2, *F* and G), thus possibly indicating that cell-surface adsorption is the first rate-limiting step in cellular internalization of VP22-GFP.

The role of GAG in cell-surface adsorption and internalization of the TAT peptide may differ from that of VP22-GFP. The TAT peptide that enters pgsD-677 cells is 40% as much as that of wild-type cells, and TAT-Cre internalization is significantly inhibited by chondroitin sulfates B and C (12, 13).

TABLE 1

List of caveola-independent lipid raft-mediated endocytic pathways

+, dependent or regulated; −, independent; CHO, Chinese hamster ovary; GPI-APs, glycosylphosphatidylinositol-anchored proteins; M2mAChR, M2 muscarinic acetylcholine receptor; CPE, carboxypeptidase E; SV40, simian virus 40; CavDC, caveolin-1-deficient cells; CTB, cholera toxin subunit B; $Cav^{-/-}$ MEFs, caveolin-1-null mouse embryonic fibroblasts; IL-2R, interleukin-2 receptor.

	Cells	Dynamin	Rho family GTPases	Rac1	RhoA	Cdc42	Arf6	Tyrosine kinases	Ref.
Group I									
VacA	HeLa, AGS	−	+	−	−	+	−	−	69
Dextran	CHO	−	+	−	−	+		+	57
GPI-APs	CHO, COS	−	+	−	−	+			59
M2mAChR	HeLa	−					+		70
CD59	HeLa	−					+		32
CPE	Neuro2A	−					+		71
SV40	CavDC	−					−	+	67
CTB	$Cav^{-/-}$ MEFs	−					−		68
Group II									
IL-2R	YT, L$\alpha\beta\gamma$	+	+	+	+				42
IL-2R	CHO	+	+		+	−		+	57
Albumin	CHO	+	+		+	−		+	57
Group III									
VP22-GFP	HeLa	+	−	−	−	−	+	−	This work

However, Fig. 2*B* shows that inhibition of VP22-GFP internalization was hardly inhibited at all by chondroitin sulfate addition to the culture medium.

In TAT-PTD, all 8 basic amino acids are equally required for cellular uptake activity (39). Our mutational analysis of VP22 (Fig. 2*F*) indicated that the roles of basic amino acids (23 of 142 amino acids) of VP22.C1 in cellular VP22-GFP internalization differ significantly depending on amino acid position. Arg-164 in VP22 is almost indispensable for VP22-GFP internalization activity, whereas other amino acids may be only moderately or slightly necessary. Thus, a long PTD such VP22.C1 may differ in the GAG interaction mode from short peptide-type PTDs such as TAT-PTD. In the former, the amino acid sequence itself appears to be much more important than the presence or absence of any positive charge. No or little similarity is found between the VP22 amino acid sequence around position 164 and the consensus amino acid sequences for heparin/heparan sulfate-binding domains so far identified (65).

Not only specific receptors but also heparan sulfate coreceptors have been shown to be required for cell-surface binding of morphogens such as Hedgehog, bone morphogenetic protein, Wnt, and fibroblast growth factors (66). Our results in Fig. 2*D* also support the notion that cell-surface VP22-GFP binding requires not only heparan sulfate but also VP22-specific receptors.

VP22-GFP May Be Internalized through a Unique Endocytic Pathway—Our results show that, in HeLa cells, VP22 is internalized through clathrin/caveola/Rho family GTPase-independent but dynamin/Arf6-dependent lipid raft-mediated endocytosis. Various clathrin- and caveola-independent and lipid raft-dependent endocytic pathways have been reported recently (10) and may be classed into two groups based on dynamin dependence (Table 1). In several cell types, cellular internalization of glycosylphosphatidylinositol-anchored proteins, simian virus 40, and cholera toxin subunit B and Arf6-Q67L-dependent internalization (32) are independent of dynamin (group I) (59, 67, 68), but dynamin is required for cellular internalization of the interleukin-2 receptor and albumin (group II) (42, 57). The former may be regulated by Cdc42 or Arf6, and the latter by RhoA and Rac1 (32, 42, 57, 59, 69–71). Our results show that VP22-GFP internalization occurs via lipid raft-mediated endocytosis dependent on dynamin and Arf6 but not Rho family GTPases such as RhoA, Rac1, and Cdc42. Thus, as summarized in Table 1, the VP22-GFP endocytic mechanism may differ significantly from those previously identified. We presume that the endocytic pathway for VP22-GFP internalization may represent the third lipid raft-mediated endocytic pathway (group III in Table 1).

VP22.C1 and short peptide-type PTDs may not have the same internalization mechanism. Indeed, short peptide-type PTDs such as TAT, the N-terminal peptide of prion protein, PDX-1, and the octaarginine peptide, in addition to their fusion proteins, are internalized via macropinocytosis (13, 14, 72–74). The TAT peptide itself is internalized via clathrin-dependent endocytosis (12), and TAT-GFP is internalized via caveola-mediated endocytosis in HeLa cells (15, 16).

Internalized VP22-GFP was also shown to be initially incorporated into EEA1-positive early endosomes (Fig. 7*A*) with transferrin incorporated via clathrin-mediated endocytosis (*D* and *H*). Internalized TAT-GFP is not incorporated into EEA1-positive early endosomes but into caveolin-1-positive structures (15, 16). This difference in the endocytic mechanism of TAT and VP22 might arise from the difference in their requirement for GAGs.

While this manuscript was being revised, Payne *et al.* (75) reported that cell-surface proteoglycans and proteoglycan-binding ligands such as cationic polymers, lipids, and polypeptides are internalized via clathrin- and caveolin-independent and flotillin- and dynamin-dependent endocytosis. This system is resistant to treatment with cholesterol-binding drugs such as filipin and nystatin and accordingly appears to be independent of lipid rafts (75). In contrast, the clathrin/caveola-independent but dynamin-dependent endocytic pathway found in VP22 internalization in this work is mediated by lipid rafts (Fig. 5), suggesting that these two systems are different from each other. In conclusion, we have shown that the mechanism of cellular uptake for VP22 is significantly different from that for short peptide-driven PTDs and that VP22 internalization is carried out via a type of lipid raft-mediated endocytosis independent of

clathrin, caveolae, and Rho family GTPases but dependent on dynamin and Arf6.

Acknowledgments—We thank K. Nakayama, J. Pessin, G. Bokoch, and J. G. Donaldson for plasmids and K. Ui-Tei for helpful discussion.

REFERENCES

1. Wadia, J. S., and Dowdy, S. F. (2002) *Curr. Opin. Biotechnol.* **13,** 52–56
2. Lindsay, M. A. (2002) *Curr. Opin. Pharmacol.* **2,** 587–594
3. Green, M., and Loewenstein, P. (1988) *Cell* **55,** 1179–1188
4. Frankel, A., and Pado, C. (1988) *Cell* **55,** 1189–1193
5. Vivès, E., Brodin, P., and Lebleu, B. (1997) *J. Biol. Chem.* **272,** 16010–16017
6. Derossi, D., Joliot, A. H., Chassaing, G., and Prochiantz, A. (1994) *J. Biol. Chem.* **269,** 10444–10450
7. Richard, J. P., Melikov, K., Vivès, E., Ramos, C., Verbeure, B., Gait, M. J., Chernomordik, L. V., and Lebleu, B. (2003) *J. Biol. Chem.* **278,** 585–590
8. Lundberg, M., Wikstrom, S., and Johansson, M. (2003) *Mol. Ther.* **8,** 143–150
9. Conner, S. D., and Schmid, S. L. (2003) *Nature* **422,** 37–44
10. Kirkham, M., and Parton, R. G. (2005) *Biochim. Biophys. Acta* **1745,** 273–286
11. Tyagi, M., Rusnati, M., Presta, M., and Giacca, M. (2001) *J. Biol. Chem.* **276,** 3254–3261
12. Richard, J. P., Melikov, K., Brooks, H., Prevot, P., Lebleu, B., and Chernomordik, L. V. (2005) *J. Biol. Chem.* **280,** 15300–15306
13. Wadia, J. S., Stan, R. V., and Dowdy, S. F. (2004) *Nat. Med.* **10,** 310–315
14. Kaplan, I. M., Wadia, J. S., and Dowdy, S. F. (2005) *J. Controlled Release* **102,** 247–253
15. Fittipaldi, A., Ferrari, A., Zoppe, M., Arcangeli, C., Pellegrini, V., Beltram, F., and Giacca, M. (2003) *J. Biol. Chem.* **278,** 34141–34149
16. Ferrari, A., Pellegrini, V., Arcangeli, C., Fittipaldi, A., Giacca, M., and Beltram, F. (2003) *Mol. Ther.* **8,** 284–294
17. Jones, S. W., Christison, R., Bundell, K., Voyce, C. J., Brockbank, S. M., Newham, P., and Lindsay, M. A. (2005) *Br. J. Pharmacol.* **145,** 1093–1102
18. Vendeville, A., Rayne, F., Bonhoure, A., Bettache, N., Montcourrier, P., and Beaumelle, B. (2004) *Mol. Biol. Cell* **15,** 2347–2360
19. Potocky, T. B., Menon, A. K., and Gellman, S. H. (2003) *J. Biol. Chem.* **278,** 50188–50194
20. Fischer, R., Kohler, K., Fotin-Mleczek, M., and Brock, R. (2004) *J. Biol. Chem.* **279,** 12625–12635
21. Elliott, G. D., and Meredith, D. M. (1992) *J. Gen. Virol.* **73,** 723–726
22. Elliott, G., and O'Hare, P. (1997) *Cell* **88,** 223–233
23. Kueltzo, L. A., Normand, N., O'Hare, P., and Middaugh, C. R. (2000) *J. Biol. Chem.* **275,** 33213–33221
24. Normand, N., van Leeuwen, H., and O'Hare, P. (2001) *J. Biol. Chem.* **276,** 15042–15050
25. Stroh, C., Held, J., Samraj, A. K., and Schulze-Osthoff, K. (2003) *Oncogene* **22,** 5367–5373
26. Brewis, N. D., Phelan, A., Normand, N., Choolun, E., and O'Hare, P. (2003) *Mol. Ther.* **7,** 262–270
27. Zavaglia, D., Normand, N., Brewis, N., O'Hare, P., Favrot, M. C., and Coll, J. (2003) *Mol. Ther.* **8,** 840–845
28. Boenicke, L., Chu, K., Pauls, R., Tams, C., Kruse, M. L., Kurdow, R., Schniewind, B., Bohle, A., Kremer, B., and Kalthoff, H. (2003) *J. Mol. Med.* **81,** 205–213
29. Narita, K., Choudhury, A., Dobrenis, K., Sharma, D. K., Holicky, E. L., Marks, D. L., Walkley, S. U., and Pagano, R. E. (2005) *FASEB J.* **19,** 1558–1560
30. Kasai, K., Shin, H. W., Shinotsuka, C., Murakami, K., and Nakayama, K. (1999) *J. Biochem.* (*Tokyo*) **125,** 780–789
31. Steiner, P., Floyd Sarria, J. C., Glauser, L., Magnin, S., Catsicas, S., and Hirling, H. (2002) *J. Cell Biol.* **157,** 1197–1209
32. Naslavsky, N., Weigert, R., and Donaldson, J. G. (2004) *Mol. Biol. Cell* **15,** 3542–3552
33. Naito, Y., Yamada, T., Ui-Tei, K., Morishita, S., and Saigo, K. (2004) *Nucleic Acids Res.* **32,** W124–W129
34. Ui-Tei, K., Zenno, S., Miyata, Y., and Saigo, K. (2000) *FEBS Lett.* **479,** 79–82
35. Summerford, C., and Samulski, R. J. (1998) *J. Virol.* **72,** 1438–1445
36. Tang, Y., and DeFranco, D. B. (1996) *Mol. Cell. Biol.* **16,** 1989–2001
37. Esko, J. D., Stewart, T. E., and Taylor, W. H. (1985) *Proc. Natl. Acad. Sci. U. S. A.* **82,** 3197–3201
38. Lidholt, K., Weinke, J. L., Kiser, C. S., Lugemwa, F. N., Bame, K. J., Cheifetz, S., Massague, J., Lindahl, U., and Esko, J. D. (1992) *Proc. Natl. Acad. Sci. U. S. A.* **89,** 2267–2271
39. Wender, P. A., Mitchell, D. J., Pattabiraman, K., Pelkey, E. T., Steinman, L., and Rothbard, J. B. (2000) *Proc. Natl. Acad. Sci. U. S. A.* **97,** 13003–13008
40. van der Bliek, A. M., Redelmeier, T. E., Damke, H., Tisdale, E. J., Meyerowitz, E. M., and Schmid, S. L. (1993) *J. Cell Biol.* **122,** 553–563
41. Oh, P., McIntosh, D. P., and Schnitzer, J. E. (1998) *J. Cell Biol.* **141,** 101–114
42. Lamaze, C., Dujeancourt, A., Baba, T., Lo, C. G., Benmerah, A., and Dautry-Varsat, A. (2001) *Mol. Cell* **7,** 661–671
43. Sauvonnet, N., Dujeancourt, A., and Dautry-Varsat, A. (2005) *J. Cell Biol.* **168,** 155–163
44. Wang, L. H., Rothberg, K. G., and Anderson, R. G. (1993) *J. Cell Biol.* **123,** 1107–1117
45. Motley, A., Bright, N. A., Seaman, M. N., Margaret S., and Robinson, M. S. (2003) *J. Cell Biol.* **162,** 909–918
46. Hinrichsen, L., Harborth, J., Andrees, L., Weber, K., and Ungewickell, E. J. (2003) *J. Biol. Chem.* **278,** 45160–45170
47. Jackson, A. L., and Linsley, P. S. (2004) *Trends Genet.* **20,** 521–524
48. Simons, K., and Ikonen, E. (1997) *Nature* **387,** 569–572
49. Martinho, R. G., Castel, S., Urena, J., Fernandez-Borja, M., Makiya, R., Olivecrona, G., Reina, M., Alonso, A., and Vilaro, S. (1996) *Mol. Biol. Cell* **7,** 1771–1788
50. Nabi, I. R., and Le, P. U. (2003) *J. Cell Biol.* **161,** 673–677
51. Pelkmans, L., and Helenius, A. (2002) *Traffic* **3,** 311–320
52. Robert, G. P., and Richards, A. A. (2003) *Traffic* **4,** 724–738
53. Gauthier, N. C., Ricci, V., Gounon, P., Doye, A., Tauc, M., Poujeol, P., and Boquet, P. (2004) *J. Biol. Chem.* **279,** 9481–9489
54. Pelkmans, L., Kartenbeck, J., and Helenius, A. (2001) *Nat. Cell Biol.* **3,** 473–483
55. Nichols, B. J. (2002) *Nat. Cell Biol.* **4,** 374–378
56. Pelkmans, L., Puntener, D., and Helenius, A. (2002) *Science* **296,** 535–539
57. Cheng, Z. J., Singh, R. D., Sharma, D. K., Holicky, E. L., Hanada, K., Marks, D. L., and Pagano, R. E. (2006) *Mol. Biol. Cell* **17,** 3197–3210
58. Wennerberg, K., Rossman, K. L., and Der, C. J. (2005) *J. Cell Sci.* **118,** 843–846
59. Sabharanjak, S., Sharma, P., Parton, R. G., and Mayor, S. (2002) *Dev. Cell* **2,** 411–423
60. Aktories, K., and Just, I. (1995) *Trends Cell Biol.* **5,** 441–443
61. Houndolo, T., Boulay, P. L., and Claing, A. (2005) *J. Biol. Chem.* **280,** 5598–5604
62. Hashimoto, S., Hashimoto, A., Yamada, A., Kojima, C., Yamamoto, H., Tsutsumi, T., Higashi, M., Mizoguchi, A., Yagi, R., and Sabe, H. (2004) *J. Biol. Chem.* **279,** 37677–37684
63. Ghosh, R. N., and Maxfield, F. R. (1995) *J. Cell Biol.* **128,** 549–561
64. Stenmark, H., Parton, R. G., Steele-Mortimer, O., Lutcke, A., Gruenberg, J., and Zerial, M. (1994) *EMBO J.* **13,** 1287–1296
65. Capila, I., and Linhardt, R. J. (2002) *Angew. Chem. Int. Ed. Engl.* **41,** 390–412
66. Filmus, J., and Selleck, S. B. (2001) *J. Clin. Investig.* **108,** 497–501
67. Damm, E. M., Pelkmans, L., Kartenbeck, J., Mezzacasa, A., Kurzchalia, T., and Helenius, A. (2005) *J. Cell Biol.* **168,** 477–488
68. Kirkham, M., Fujita, A., Chadda, R., Nixon, S. J., Kurzchalia, T. V., Sharma, D. K., Pagano, R. E., Hancock, J. F., Mayor, S., and Parton R. G. (2005) *J. Cell Biol.* **168,** 465–476
69. Gauthier, N. C., Monzo, P., Kaddai, V., Doye, A., Ricci, V., and Boquet, P. (2005) *Mol. Biol. Cell* **16,** 4852–4866
70. Delaney, K. A., Murph, M. M., Brown, L. M., and Radhakrishna, H. (2002) *J. Biol. Chem.* **277,** 33439–33446

71. Arnaoutova, I., Jackson, C. L., Al-Awar, O. S., Donaldson, J. G., and Loh, Y. P. (2003) *Mol. Biol. Cell* **14,** 4448–4457
72. Magzoub, M., Sandgren, S., Lundberg, P., Oglecka, K., Lilja, J., Wittrup, A., Göran Eriksson, L. E., Langel, U., Belting, M., and Gräslund, A. (2006) *Biochem. Biophys. Res. Commun.* **348,** 379–385
73. Noguchi, H., Matsumoto, S., Okitsu, T., Iwanaga, Y., Yonekawa, Y., Nagata, H., Matsushita, M., Wei, F. Y., Matsui, H., Minami, K., Seino, S., Masui, Y., Futaki, S., and Tanaka, K. (2005) *Cell Transplant.* **14,** 637–645
74. Nakase, I., Niwa, M., Takeuchi, T., Sonomura, K., Kawabata, N., Koike, Y., Takehashi, M., Tanaka, S., Ueda, K., Simpson, J. C., Jones, A. T., Sugiura, Y., and Futaki, S. (2004) *Mol. Ther.* **10,** 1011–1022
75. Payne, C. K., Jones, S. A., Chen, C., and Zhuang, X. (2007) *Traffic* **8,** 389–401